Fuel 239 (2019) 737–746

Contents lists available at ScienceDirect

Fuel

journal homepage: www.elsevier.com/locate/fuel

Full Length Article

Performance of metal-functionalized rice husk cellulose for CO_2 sorption and CO_2/N_2 separation

Sarah Campbell[a], Franciele L. Bernard[c], Daniela M. Rodrigues[b], Marisol F. Rojas[e,f], Luz Ángela Carreño[f], Vitaly V. Chaban[g], Sandra Einloft[b,d,*]

[a] Faculty of Science, Agriculture & Engineering-Newcastle University, NE1 7RU, United Kingdom
[b] Post-Graduation Program in Materials Engineering and Technology, Pontifical Catholic University of Rio Grande do Sul – PUCRS, Brazil
[c] School of Science, Pontifical Catholic University of Rio Grande do Sul – PUCRS, Brazil
[d] School of Technology, Pontifical Catholic University of Rio Grande do Sul – PUCRS, Brazil
[e] School of Science and Engineering, Universidad de los Llanos, Km 12 Vía Puerto López, Villavicencio, Colombia
[f] School of Chemistry, Universidad Industrial de Santander, Street 9, 27, Bucaramanga, Colombia
[g] P.E.S, Vasilievsky Island, Saint Petersburg Leningrad Oblast, Russian Federation

ARTICLE INFO

Keywords:
CO_2 capture
Metal-functionalized celulose
CO_2/N_2 separation

ABSTRACT

In this work, cellulose was extracted from rice husk. Fe_3O_4 and TiO_2 particles were successfully bonded on the cellulose surface via hydroxyl group. The products were confirmed and characterized by Fourier transform infrared spectroscopy (FTIR), thermogravimetric analysis (TGA), scanning electron microscopy (SEM), X-ray diffraction (XRD) and X-ray photoelectron spectroscopy (XPS). A pressure decay technique was carried out to evaluate CO_2 sorption capacity and reusability. In addition, ab Initio calculations were performed. The experimental results show an increase in CO_2 sorption ability upon cellulose modification with metal oxides. Titanium dioxide modified cellulose fibers (cellulose-TiO_2, 184.1 mg/g at 30 bar and 298.15 K) and iron oxide modified cellulose fibers (cellulose-Fe_3O_4, 130.6 mg/g at 30 bar and 298.15 K) exhibited enhanced CO_2 uptake than nonmodified cellulose (cellulose, 81.6 mg/g under the same conditions). The best CO_2/N_2 selectivity result was obtained for cellulose-TiO_2 (3.56 ± 0.16). Selective capacity of cellulose-TiO_2 for CO_2/N_2 was approximately 270% higher than raw cellulose fibers. CO_2 sorption recycling experiments demonstrated high stability and reuse capacity in CO_2 capture processes of Cellulose-TiO_2.

1. Introduction

Excessive carbon dioxide production is the largest contributor to global warming of anthropic origin [1]. CO_2 is consistently produced in excess through various human activity [1,2]. As a potential method to counteract the serious environmental threat of global warming, reduction of CO_2 is of serious interest to scientists worldwide [1]. Technologies for carbon capture and storage (CCS) have been widely studied as a viable method to reduce carbon emissions and mitigate the climate change effect [2–4]. Research into CO_2 sorption and separation is currently being carried out in a wide variety of areas. Zeolites [5,6], amine technology [7–9], silica [10], silica gel [11,12], mesoporous materials [13,14], poly (ionic liquid)s [15], metal organic frameworks [16–18], chemical looping [19], lithium-based ceramics [20] and cellulose [21,22] all provide a potential solution to the ever-growing CO_2 problem. One area of particular interest is the modification of cellulose to enhance its adsorptive properties. Cellulose is the most abundant organic polymer on earth [23], present in the structure of all plant cell walls. Rice husk is composed of cellulose (35%), hemicellulose (25%), lignin (20%), crude protein (3%) and ash (17%) [24] An estimated of 500 million tons per year of rice crop is produced worldwide [21]. Isolation from the rice husk waste generated from the cereal process [25,26] can provide an attractive, low cost method of producing cellulose [22]. Following this, it could provide an efficient base method to produce cellulose related CO_2 adsorptive compounds. As well as being abundant and readily available, cellulosés non-toxicity, resistance and the fact that its surface can be modified by chemical treatments make it an attractive candidate for CO_2 sorption [21,22]. Hydroxyl groups can be deprotonated readily, which allows for the application of a variety of reaction mechanisms involving the highly reactive O^- group [27–31]. These reaction pathways can alter or enhance certain properties of cellulose, allowing for the production of new, cost-effective materials

* Corresponding author.
E-mail address: Einloft@pucrs.br (S. Einloft).

https://doi.org/10.1016/j.fuel.2018.11.078
Received 28 August 2018; Received in revised form 15 November 2018; Accepted 17 November 2018
Available online 29 November 2018

with an increased selectivity for certain applications.

The presence of basic sites on the surface of transition metal oxides, such as Fe_3O_4 and TiO_2, make them an interesting candidate for enhancing the CO_2 sorption of certain compounds. This is due to the acidic nature of CO_2. This acid-base attraction could enhance the adsorptive properties of cellulose. A few previous studies suggest Fe_3O_4 has potential in adsorption technology. A study on the adsorption behaviors of iron oxide on a mesoporous compound MCM-414 [32] showed that the CO_2 sorption capacity of the mesoporous compound increases with the addition of iron oxide, partly due to the transfer of electrons from the metal d orbital to the CO_2 antibonding orbital. A density functional theory study on the interaction of CO_2 with Fe_3O_4 (1 1 1) surface [33] shows the same, with adsorption of CO_2 onto Fe_3O_4 occurring due to this Lewis acid-base interaction. This leads to the formation of a covalent bond between CO_2 and Fe_3O_4. The tendency of Fe_3O_4 to aggregate limits its applicability in the field of adsorption technologies due to the limitation of the exposed surface [34]. Dispersing the magnetite particles onto a solid matrix, such as cellulose, could reduce this aggregation and enhance the adsorptive properties of the metal oxide. Past studies on the adsorption potential of TiO_2 [35,36] suggest the addition of TiO_2 into a complex can enhance the adsorptive properties. A study performed on the interaction of CO_2 on rutile TiO_2 (1 1 0) surfaces [37] investigates further into how CO_2 can be physisorbed onto the TiO_2 surface. As well as previous studies indicating the increase in adsorption relating to TiO_2, the addition of TiO_2 to the cellulose matrix leads to an increase in surface area of the complex [32].

The methods of cellulose modification carried out in this work are implemented with environmental caution in mind. The Fe_3O_4 modification method [28] involves the addition of magnetite particles across cellulose with virtually no produced waste. The addition of TiO_2 to cellulose [38] uses a NaOH/urea solvent dissolution process which is a new, green approach to this procedure.

This is an innovative area of research due to several key factors – including cellulose's natural abundancy and the many potential applications these transition metals have in adsorption technology. Furthermore, there have been very few studies on their potential adsorptive properties. In this work, cellulose fibers extracted from rice husk were modified using both Fe_3O_4 and TiO_2 nanoparticles; their CO_2 sorption capacity was evaluated. To the knowledge of the authors research in this area has not been carried out before.

2. Experimental

2.1. Materials

The rice husks were donated by Cooperativa Arrozeira Extremo Sul Ltda. The rice husk was washed with distilled water and dried in an oven at 100 °C for 8 h. The dried husk was grounded in a knife mill. The product was collected. Sodium hydroxide (NaOH, 97% Vetec), hydrogen peroxide (H_2O_2, 35%, Neon), sulphuric acid (H_2SO_4, F. Maia, P. A), ferric chloride hexahydrate ($FeCl_3{\cdot}H_2O$, 97%, Sigma-Aldrich), sodium bicarbonate ($NaHCO_3$, Dinâmica), ascorbic acid (C_6H_80, Vetec), urea (40%, Sigma-Aldrich), acetic acid (CH_3COOH, 99.7%, Sigma-Aldrich), nitric acid (HNO_3, 65%, Vetec), ethanol (C_2H_5OH, 99.5%, Sigma-Aldrich), toluene (C_7H_8, 99.5%, Vetec) and ethyl ether $(C_2H_5)_2O$, 99.9%, Sigma-Aldrich) were used as purchased. Tetra-n-butyl-titanate ($C_{16}H_{32}O_4Ti$) (99%, Acros).

2.2. Cellulose extraction

The cellulose fibers extraction procedure was adapted from literature [22,39]. An alkaline treatment was carried out on the rice husk (50 g) using 4%wt NaOH (400 mL) for 2 h at 90 °C under reflux with continuous stirring. Following this, an acid hydrolysis treatment was carried out on the material using 5 mol/L H_2SO_4 (400 mL) under reflux with continuous stirring at room temperature. Afterward, a bleaching treatment was carried out on the fibers by addition of 16%wt H_2O_2 (200 mL) and 5%wt NaOH (200 mL) at 55 °C with continuous stirring. After each treatment, the material was washed with distilled water until neutral pH (5–7), filtered and dried in oven for 24 h at 100 °C. Purity test details are well reported in Technical Association of Pulp and Paper Industry (TAPPI standard T203 OS-74). Purity tests performed resulted in 82% of cellulose.

2.3. Cellulose modification with Fe_3O_4

First, magnetite particles were prepared using a co-precipitation method adapted from literature [28]. $FeCl_3{\cdot}6H_2O$ (0.46 g) was dissolved in deionized water (12.5 mL). Then, $NaHCO_3$ (6%) was added to the solution dropwise until a precipitate formed. Ascorbic acid (0.06 g) was added and the mixture was kept under nitrogen atmosphere and stirring for 15 min, then completed to 25 mL with deionized water. The freshly prepared magnetite particles (25 mL) were added to a suspension of nanocellulose in deionized water (10 g/500 mL) under nitrogen with continuous stirring at room temperature for 24 h. The products were filtered, washed with deionized water and dried in oven.

2.4. Cellulose modification with TiO_2

This modification method was taken from literature [38]. A cellulose solution was prepared by addition of cellulose (1.62 g) to a 7:12% wt NaOH/urea solution (50 mL) under stirring at room temperature. The suspension was immediately cooled in freezer to −12 °C for 12 h. A mixture of tetra-n-butyl titanate (25 mL) and the previously prepared cellulose suspension (50 mL) were poured into a 100 mL Teflon-lined stainless steel autoclave and kept at 180 °C for 24 h. The product was centrifuged until a clear liquid was obtained, washed with ethanol and dried in oven at 60 °C.

2.5. Characterization

Fourier Transform Infrared analysis of the samples was recorded using the KBr pellet method on a Perkin-Elmer Spectrum 100 FT-IR Spectrometer with a wavenumber range 4000–400 cm^{-1}. Thermal analysis was carried out using TA Instruments SDT-Q600 with a heating rate of 10 °C/min and a temperature range of 20–600 °C under nitrogen atmosphere. SEM was carried out using FEI Inspect F50 equipment in secondary electrons (SE) mode. Chemical composition was evaluated by energy dispersion X-ray spectrometry (EDS). For this purpose, samples were covered with a thin layer of gold. Experiments by X-ray photoelectron spectroscopy (XPS) were carried out with XPS/ISS/UPS-ACenteno surface characterization platform built by SPECS (Germany). The platform is equipped with PHOIBOS 150 2D-DLD energy analyzer. A monochromatic Al Kα X-ray source (FOCUS 500) operated at 200 W was used for measurements. The pass-through energy of the hemispherical analyzer was set at 100 eV for the general spectra and 60 eV for high-resolution spectra. The surface charge compensation was monitored with a Flood Gun device (FG 15/40-PS FG500) operated at 58 μA and 2 eV. High-resolution spectra of the elements found were recorded for quantification, CasaXPS software was used for spectral analysis and curve fitting using C–C signal position at 284.6 eV as Ref. [40]. X-ray powder diffraction patterns were recorded using a Bruker-AXS D8 ADVANCE diffractometer operated at 40 kV voltage and 20 mA current with Cu Kα radiation (λ = 1.5406 Å), 3–80° range with 0.02 step and 1.0°/min scanning time. Segal method (Eq. (1)) was used to calculate the crystallinity index of the materials (CrI) [41].

$$Crl = \frac{I_{002} - I_{AM}}{I_{002}} * 100 \quad (1)$$

where I_{002} is maximum intensity of the 002 peak and I_{AM} is intensity scattered by the amorphous part of the sample. The diffraction peak for

plane (0 0 2) is located at diffraction angle around 2θ = 22° and intensity scattered by the amorphous part is measured as the lowest intensity at diffraction angle around 2θ = 18° [39].

2.6. CO_2 sorption measurements

A pressure decay technique was carried out using a dual-chamber gas sorption cell [42] which was equipped with an Edwards RV5 vacuum pump and placed inside a thermostatic oil bath at 25 °C (298.15 K). A detailed description of sorption apparatus can be found in our previous works [21,43]. 0.7 g-1 g of sample was weighed and placed inside the sorption chamber, then subjected to a 10^{-3} mbar vacuum for one hour. CO_2 (air liquid/99.998%) was then admitted into the reservoir at desired pressures. The CO_2 sorption capacity was calculated using Eqs. (2) and (3).

$$n_{CO2} = \frac{p_i V_{gc}}{Z_{(P_i,T_i)} R T_i} - \frac{p_{eq}(V_t V_p)}{Z_{(p_{eq},T_{eq})} R T_{eq}} \tag{2}$$

$$w_{CO2/g} = \frac{n_{CO2} M}{W_s} \tag{3}$$

where $w_{CO2/g}$ = gas mas adsorbed in the sample, p_i and T_i = pressure and temperature in the gas chamber, p_{eq} and T_{eq} = pressure and temperature at equilibrium, V_{gc} = volume of the gas chamber, V_p = volume of the sample, V_t = total volume of the sorption cell and Z = the coefficient of compressibility calculated using Span-Wagner equations-of-state for CO_2 [44].

2.7. Sorption/desorption experiments

Sorption/desorption experiments used CO_2. Seven CO_2 sorption/desorption cycles were performed on the modified cellulose fibers. CO_2 sorption was evaluated at 25 °C (298.15 K) and 2 MPa with desorption following each cycle by vacuum (10^{-3} mbar) at 298.15 K during 1 h.

2.8. CO_2/N_2 separation selectivity

The CO_2/N_2 selectivity experiments were also performed in a dual-chamber gas sorption cell similar to Koros et al [42]. In the test, samples (1.0–1.5 g) were previously degassed under vacuum (10^{-3} mbar) at 298.15 K during 1 h. The tests were conducted using a binary mixture (15.89 mol % of CO_2 and N_2 balance) at 298.15 K and 2 MPa. The apparatus and complete experimental procedure were described elsewhere [10,45,46]. CO_2 selectivity over N_2 is calculated from the mole fractions in the gas phase (Y_i) and in the adsorbed phase (X_i), as shown in Eq. (4):

$$S = \frac{X_{CO_2}/Y_{CO_2}}{X_{N_2}/Y_{N_2}} \tag{4}$$

2.9. Molecular modeling

Ab initio calculations were conducted in this work to rationalize experimental observations of CO_2 capture. We employed the M11 exchange-correlation density functional based on the meta-GGA approximation, i.e. includes terms depending on kinetic energy density [47]. The final form of the employed exchange-correlation functional accounts for high-quality benchmark databases and provides satisfactory results in most cases, where calculation vs. experiment comparison is possible. The Los Alamos double-zeta LANL2DZ basis set with core potentials [48] was used to construct wave functions of the systems. The wave energetic function convergence criterion was set to 10^{-7} Hartree. The internal forces were minimized in accordance with the steepest descent algorithm. The procedure was repeated until the energy difference between two consequent molecular configurations became smaller than 1 kJ mol^{-1}, assuming negligible immediate forces on each atomic nucleus.

For each system, the strongest atom–atom attraction (CO_2 – sorbent) was identified and the corresponding distance was increased stepwise (0.3 nm) to sample the phase space in the vicinity of the sorbent surface. Upon distance increase, only a single selected distance per molecular system was constrained, whereas all other components of the Z-matrix were allowed to adapt to the changes introduced (relaxed potential energy scan). In total, 1848 single-point calculations (self-consistent field wave function optimizations) were performed to derive potential curves.

The most energetically favorable configurations of the systems were obtained via full unconstrained optimization. Each reported adsorption energy already includes empirical van der Waals correction [49]. All calculations discussed below were performed in GAMESS 2014 along with in-home codes including certain scipy.org functions [50]. Initial geometries of the simulated systems are shown in Fig. 7.

3. Results and discussion

The hydroxyl groups in cellulose favor the hydrogen bond formation [51], providing an alternate bonding interaction for complex formation. These aforementioned bonding interactions allow for the dispersion of the transition metal oxides used in this work, Fe_3O_4 and TiO_2, across cellulose. Previous investigation into this area suggests TiO_2 is held on the cellulose surface either by the hydroxyl groups acting as Lewis basic sites to form a titanium complex [52,53] or through hydrogen bonding and Van der Waal forces [52]. Cellulose-Fe_3O_4 complexes are bound solely by hydrogen bonds [54] and Van der Waal forces [54,55].

The FTIR of all compounds is displayed in Fig. 1. The FTIR spectrum of cellulose (Fig. 1a.) displays all characteristic bands [22,39,56,57]. The broad peak at 3446 cm^{-1} can be attributed to hydrogen bonded –OH stretching. –CH_2 and –CH_3 stretching vibrations are shown by band 2895 cm^{-1}. The 1635.5 cm^{-1} band is representative of moisture in the cellulose. The band at 1430 cm^{-1} is assigned to a symmetric –CH_2 bending vibration. –OH bending is shown by the 1369 cm^{-1} band. C–O–C asymmetric bridge stretching is represented by the band at 1100 cm^{-1}. Absorption bands at 1060 cm^{-1} and 890 cm^{-1} observed in the spectrum refer to the C–H and C–O stretching of the cellulose structure. The lack of adsorption band at ~1700 cm^{-1} indicates there is little or no hemicellulose and lignin impurities present in the sample [57,58].

FTIR spectrum of cellulose-Fe_3O_4 (Fig. 1b.) showed appearance of a band at 478 cm^{-1} due to the Fe-O bonding stretch in magnetite [58,59]. Another significant peak for magnetite is present at 1635.5 cm^{-1} [28]. In this case, there is an overlap with the cellulose peak relating to moisture, so it cannot be distinguished. Shifting in the –OH band from 3446 cm^{-1} to 3421 cm^{-1} indicates a bonding interaction between hydroxyl groups and magnetite. This supports the theory that magnetite is incorporated onto the surface via hydrogen bonds as hydrogen bonding weakens the OH band.

For the FTIR spectrum of cellulose-TiO_2 (Fig. 1c.), the differences are slightly more pronounced. The introduced intense band at 673.37 cm^{-1} is due to anatase TiO_2 [38]. The broad adsorption band at 474.56 cm^{-1} can be attributed to the Ti-O-Ti stretching vibrations [60]. Shifting in –OH band from 3446 cm^{-1} to 3414 cm^{-1} and a weakening in band intensity indicates interaction between hydroxyl group and titanium. Shift corresponding to O=C vibration 1635.5 cm^{-1} to 1630 cm^{-1} indicates Ti–O–C vibration. 2910 cm^{-1} band disappearance in agreement with literature and could be due to the blocking of C–H in-plane stretching caused by the steric hindrance TiO_2 creates in the molecule [61].

Surface composition analysis was done through survey and high-resolution XPS spectra of all cellulose compounds. The XPS survey spectra is displayed in Fig. 2. The elemental composition and percentage is shown in Table 1. High resolution C 1s and O 1s data is shown in

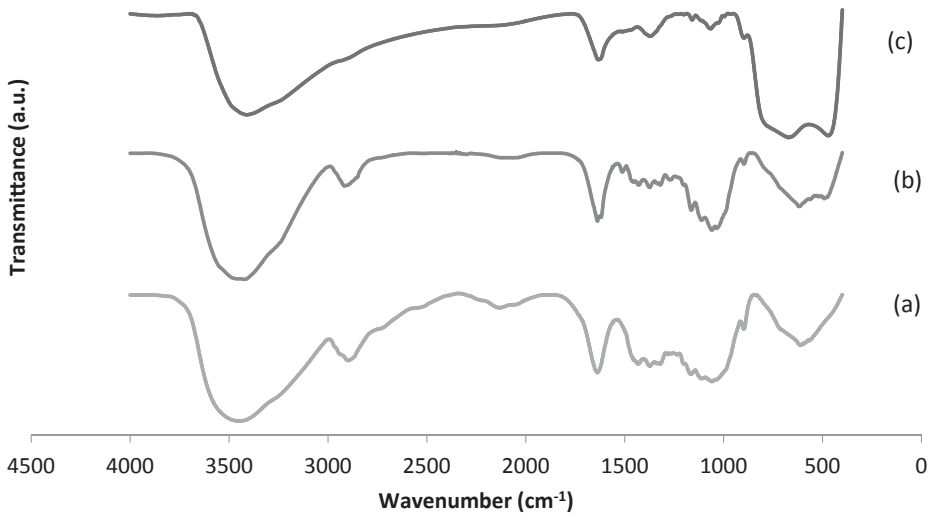

Fig. 1. FTIR spectra of materials: (a) cellulose, (b) cellulose-Fe3O4 and (c) cellulose-TiO_2.

Table 2. The experimental C:O ratio of cellulose 1.76. The true C:O ratio of cellulose is 1.2 [62]. This suggests the presence of hemicellulose and/or lignin impurities. The small amount of nitrogen present is due to the remaining crude protein in the sample. The silicon presence is due to the small amount of SiO_2 present in rice husk [63]. The cellulose C 1s spectrum shows the characteristic peaks of cellulose [21,64]. Peaks centered at 285.28 eV (C2) are due to the C–O and C–H/C–C bonds. This peak can also be assigned to the C–N bond in the crude protein contaminant. The peaks at 287.18 eV (C3) and 288.9 eV (C4) are representative of the O–C–O/C=O and O–C=O bonds, respectively. The C1 value in C 1s spectra is representative of carbon atoms with zero neighboring oxygen atoms. Pure cellulose has a C1 value of 0 [21]. The tabulated value of 7.95at.% at 283.25 eV represents the hemicellulose and lignin impurities present in the sample. The low value suggests a small amount present, which agrees with the tested purity value of 82% and the absence of a lignin band in the FTIR spectra (Fig. 1.). The cellulose O 1 s spectrum shows peaks at 531.20 eV (O3) and 533.56 (O4) corresponding to C=O and C–O bonds, respectively, from lignin and cellulose.

Table 1
Surface composition and elemental ratio of cellulose and modified cellulose from XPS survey spectra.

Sample	Surface composition (at.%)								Elemental ratio
	C	O	N	Si	Fe	Na	Ti	Cl	C/O
Cellulose	63.1	35.8	0.5	0.7					1.76
Cellulose-Fe_3O_4	61.8	36.8	0.4		0.4	0.6			1.68
Cellulose-TiO_2	27.7	46.1	0.4			9.7	15.5	0.7	0.60

The addition of magnetite to cellulose is confirmed by the XPS results. Past literature using the same synthesis method [28] reported a Fe wt.% of 4.13 using energy-dispersive X-ray spectroscopy (EDS). Converting wt.% to at.% yields a value of 0.28, similar to the compound produced in this work. The position of the Fe 2p peak at 710.3 eV agrees with literature to iron oxides [65–67]. The small amount of Na is due to the addition sodium bicarbonate in the reaction with magnetite. The disappearance of Si could possibly be due to dissolution in the alkaline

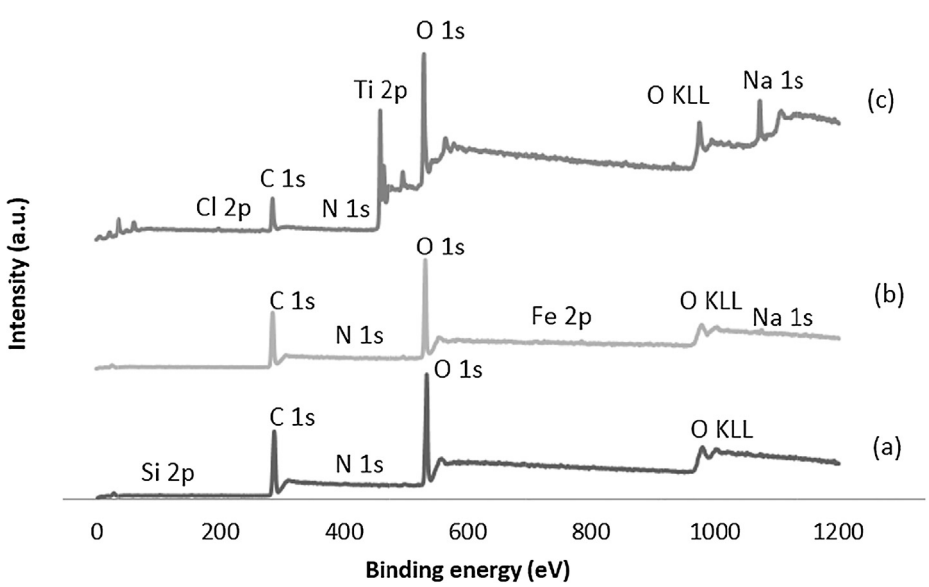

Fig. 2. XPS survey spectra of (a) cellulose, (b) cellulose-Fe_3O_4 and (c) cellulose-TiO_2.

Table 2
Carbon type and oxygen percentages in cellulose and modified cellulose from XPS high resolution spectra.

Sample	Carbon type composition (at. %)				Oxygen (at.%)			
	C1	C2	C3	C4	O1	O2	O3	O4
Cellulose	7.95	49.40	38.04	4.61			28.53	71.47
Cellulose-Fe_3O_4	9.89	55.24	30.33	4.54			43.03	56.97
Cellulose-TiO_2	10.52	70.22	11.90	7.37	5.75	72.15	14.02	8.07

sodium bicarbonate solution. The previously reported O 1s Fe_3O_4 lattice peak is ~530 eV [65,68,69]. A previous study on the nature of hydrogen in XPS [70] reported that hydrogen bonds produce a higher binding energy shift for O 1s peaks. So, the increase in the amount of oxygen peak present at 531.32 eV (O3), in relation to pure cellulose, can be assigned to the lattice oxygen, showing an energy shift upon magnetite addition. This supports the idea that magnetite is dispersed across the cellulose surface via hydrogen bonds.

In the survey spectrum of cellulose/TiO_2 was identify 15.5 at.% of Ti 2p at 458.3 eV, this binding energy is close to the pure TiO_2 (458.8 eV), showing that this one has been dispersed upon cellulose. In the high-resolution spectrum of Ti, the 464.1 eV and 458.3 eV peaks present for Ti $2p_{1/2}$ and Ti $2p_{3/2}$ respectively agree with past reports of TiO_2 XPS spectra [60], showing titanium to be in the Ti^{4+} chemical state. The C:O at.% ratio reduces from 1.76 to 0.6, due to the addition of large amounts of TiO_2. The large presence of Na is due to the NaOH/urea solution used in the synthesis of the complex. Trace amounts of Cl present unaccounted for but could be due to contaminants in the tetra-n-butyl titanate solution depending on method of preparation. The disappearance of Si is most likely due to dissolution in the highly alkaline solution. The O 1s 529.54 eV (O2) peak corresponds to the Ti–O–Ti lattice oxygen [60,71]. The 531.65 eV (O3) peak is representative of Ti–O–C [60] and the 533.64 eV (O4) peak corresponds to C–O bonding. The ratio of at.% for O 1s O4:O3 decreases from 2.5 to 0.56 upon TiO_2 addition. This supports the formation of a titanium complex via the surface hydroxyl oxygen. The small peak at 288.81 eV (O1) could be ascribed to O–H surface adsorption of water [71].

The X-ray diffraction pattern of all compounds is displayed in Fig. 3. Characteristic sharp peaks of cellulose attributed to (1 1 0), (2 0 0) and (0 0 4) can be observed at 2θ = 15.88°, 22.5° and 34.7° respectively [39,72]. In the cellulose-Fe_3O_4 spectrum (Fig. 4b) there is an absence of the reflections corresponding to magnetite. This is in agreement with previous literature [28] using the same synthesis method and is potentially a result of low magnetite content in the complex. The XRD patterns of cellulose-TiO_2 contained only reflections corresponding to TiO_2 holding an anatase structure. Peaks at 2θ = 28.24°, 40°, 48.2°, 54,9° and 63.82° are assigned to (1 0 1), (0 0 4), (2 0 0), (2 1 1) and (2 0 4) of anatase TiO_2 [38,71,73–75]. No obvious peaks of cellulose were observed, which can be attributed to the strong peak intensity of TiO_2 and is agreement with a previous study using this synthesis method [38].

Cellulose XRD graph is well defined, indicating a crystalline structure [22] (Fig. 3a). This is due to hydrogen bonding interactions and Van der Waals forces between adjacent molecules [76]. The crystallinity index (CrI) of cellulose was ca. 93.2%, whereas for the sample cellulose-Fe_3O_4 (Fig. 3b) was ca. 66,9%. The presence of Fe_3O_4 does not affect considerably the crystalline degree. This can be attributed to a low Fe_3O_4 distribution across cellulose and is in agreement with a previous study [28]. The XRD cellulose-TiO_2 pattern (Fig. 3c) displays a visible increase in amorphicity through broader peaks. The reduction in crystallinity can be attributed to formation of a cellulose titanium complex via the hydroxyl groups of cellulose. This disrupts the hydrogen bonds and Van der Waal forces between adjacent cellulose molecules, therefore disrupting the crystalline structure. This behavior indicates the idea that a significant amount of TiO_2 was loaded into cellulose structure.

Scanning electron microscopy with EDS was carried out to assess the surface topography and Chemical composition. The resulting images spectra and are displayed in Fig. 4. Cellulose displays a typical fibrous looking surface [21]. The roughness of cellulose fibers is due to rice husk impurities removal [77] which indicates a successful extraction. The cellulose assembled structure is due to hydrogen bonding between adjacent hydroxyl groups [78]. This is shown to be disrupted in cellulose-Fe_3O_4 due to the hydrogen bonding interaction between cellulose hydroxyl groups and Fe_3O_4. Both Fe_3O_4 and TiO_2 were successfully dispersed across the cellulose surface, with a much higher metal oxide

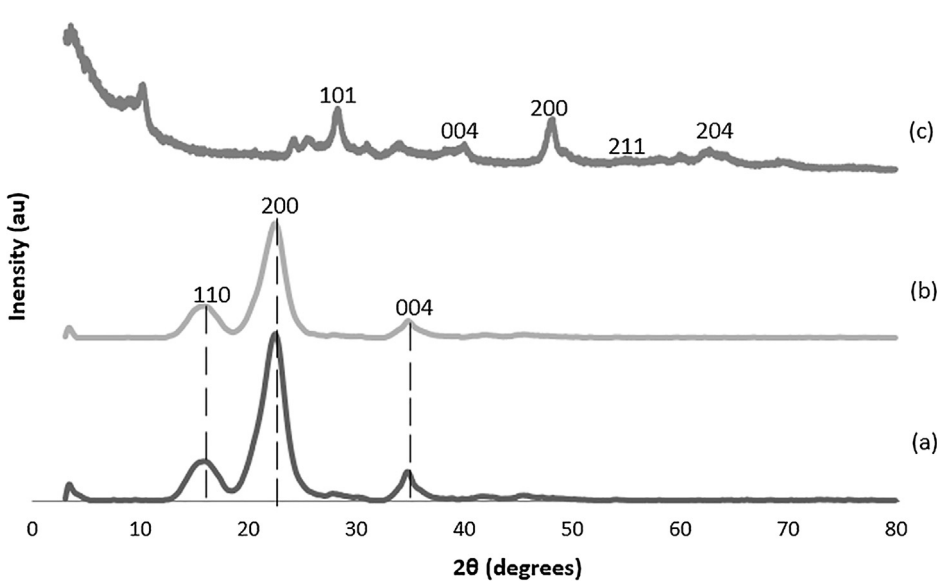

Fig. 3. XRD pattern of (a) cellulose, (b) cellulose/Fe_3O_4 and (c) cellulose/TiO_2.

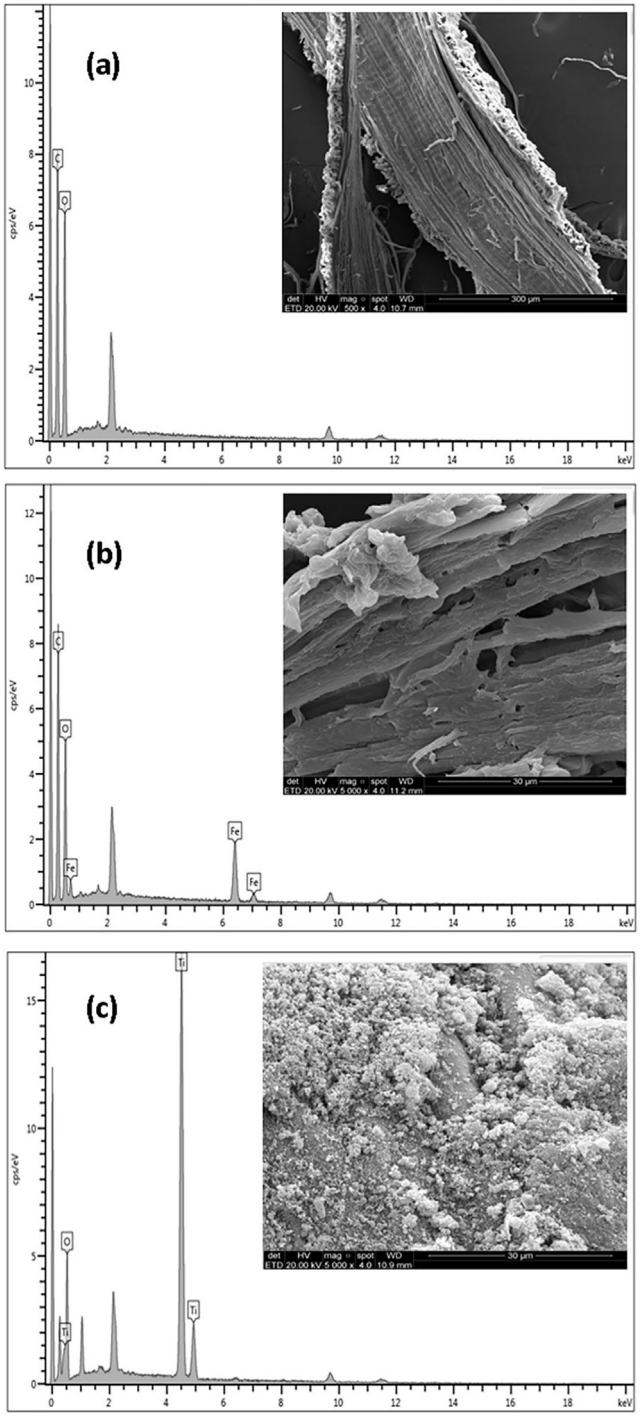

Fig. 4. Micrographs and EDS spectra of materials: (a) cellulose, (b) cellulose-Fe_3O_4, (c) cellulose- TiO_2.

loading capacity for cellulose-TiO_2. The bundles of TiO_2 are characteristic of TiO_2 holding an anatase structure [79]. EDS spectra of all samples (Fig. 4) revealed the presence of peaks corresponding to cellulose structure (C,O). EDS Analysis also showed the presence of Fe peaks in the cellulose/Fe_3O_4 and Ti peaks in cellulose/TiO_2 sample indicating that the cellulose fibers were modified with metal oxides.

Cellulose and modified cellulose thermogravimetric curves are presented in Fig. 5. Cellulose and Cellulose-Fe_3O_4 showed two thermal events. Initial weight loss inferior to 8% occurring below 100 °C is due to water vaporization [22,58].

In the second stage, cellulose-Fe_3O_4 (T_{onset} = 331.49 °C, T_{max} = 332.01 °C) has a total weight loss of 71.66%, whereas cellulose (T_{onset} = 320.36 °C, T_{max} = 352.46 °C) has a total weight loss of 75.79%. This stage is related to cellulose structure degradation [39]. Cellulose-TiO_2 thermal decomposition occurs in three stages. The first (weight loss 8%) below 100 °C is attributed to moisture loss, the second weight loss of 6.85% (T_{onset} = 153.32 °C, T_{max} = 135.5 °C) is related to titanium hydroxyl groups elimination and finally the weight loss of 3.05% correspond to cellulose degradation (T_{onset} = 339.22 °C, T_{max} = 313.72 °C) [73,80]. Residual weight percentages of cellulose, cellulose-Fe_3O_4 and Cellulose-TiO_2 were 15.40%, 16.39% and 81.07% respectively. Cellulose-Fe_3O_4 and Cellulose-TiO_2 higher residual content can be attributed to Fe_3O_4 and TiO_2, respectively [81,82].

Experimental results of CO_2 sorption for cellulose and modified cellulose are shown in Fig. 6. The overall trend shows an increase in CO_2 sorption capacity for both modified compounds, with the effect being more pronounced at higher pressures. The lower CO_2 sorption capacity value obtained for cellulose is in agreement with a previous study [21] which placed the value for cellulose as 88 mg/g at 3 MPa using the same technique.

Cellulose already has adsorptive properties due to the CO_2 affinity of the hydroxyl, ether and ester polar groups [22]. Cellulose CO_2 sorption capacity values of 81.6 mg/g at 30 bar and 37.6 mg/g at 1 bar were achieved. Addition of metal oxides to the compound provides a stronger acid-base adsorption mechanism (see Fig. 7a and b). Cellulose-Fe_3O_4 yielded values of 130.6 mg/g at 30 bar and 40.2 mg/g at 1 bar. Cellulose-TiO_2 provides the highest CO_2 sorption capacity values of 184.1 mg/g at 30 bar and 42.2 mg/g at 1 bar. Cellulose-TiO_2 presented high CO_2 sorption as compared with Pure TiO_2 (~27.3 mg/g or ~0.62 mmol/g at 298.15 K and 1 bar) [83]. Cellulose-TiO_2 potentially provides the more attractive adsorbent due to it's high sorption capacity and good thermal stability. It is difficult to compare sorption capacity between the two metal oxide compounds due to the difference in metal oxide loading (0.4at.% Fe for cellulose-Fe_3O_4, 15.5at.% Ti for cellulose-TiO_2). However, in cellulose-TiO_2 the higher sorption capacity could be a result of titanium lower electronegativity when compared to iron. This can be better explained by simulation studies (see Fig. 9). At lower pressure cellulose-TiO_2 sorption capacity was similar to the higher CO_2 sorption value reported for cellulose-based poly(ionic liquid) (PIL) CL-TBA (44.0 mg/g at 298.15 K and 1 bar) [22] and superior in relation to PIL [CelEt$_3$N][PF_6] (38.0 mg/g at 298.15 K and 1 bar) [21]. At high pressure, cellulose-TiO_2 exhibited better CO_2 sorption capacity (184.1 mgCO_2/g at 30 bar) than CL-TBA (71.0 mg/g at 298.15 K and 30 bar) [22] and [CelEt$_3$N][PF_6] (168 mg/g at 298.15 K and 30 bar) [21].

The CO_2/N_2 selectivity results for all samples are presented in Fig. 8. Cellulose showed a poor performance (selectivity is only 0.96 ± 0.15) even presenting some polar groups in the structure [84,85]. The CO_2/N_2 cellulose selectivity can be improved by Fe_3O_4 and TiO_2. Modified cellulose fibers showed higher selective in relation to non-modified cellulose. CO_2/N_2 selective capacity of cellulose-TiO_2 of 3.56 ± 0.16 is higher when compared to cellulose- Fe_3O_4 (1.77 ± 0.16). Preferential affinity of CO_2 for cellulose containing the TiO_2 rather than Fe_3O_4 is probably due to larger polarity of the Ti-O covalent bonds as observed by simulations (Fig. 9).

Cellulose-TiO_2 was selected to a CO_2 sorption study and recyclability behavior. CO_2 sorption in cellulose-TiO_2 was reversible for seven consecutive cycles. These results evidenced that titanium dioxide modified cellulose fibers have high stability and capacity of being reused in CO_2 capture processes.

The simulations confirm that although unmodified cellulose is a fairly weak CO_2 sorbent, it can be successfully reinforced with inorganic oxides, such as Fe_3O_4 and TiO_2. (Fig. 9). Compare 21 kJ mol^{-1} (pristine cellulose) to 41 kJ mol^{-1} (cellulose modified with Fe_3O_4) to 46 kJ mol^{-1} (cellulose modified with TiO_2). The non-zero performance of cellulose originates from medium-strength hydrogen bonding, r (O–H) ~ 0.20 nm, of the oxygen atom of CO_2 with one of the hydroxyl groups of cellulose. In contrast, adsorption of CO_2 on the inorganic

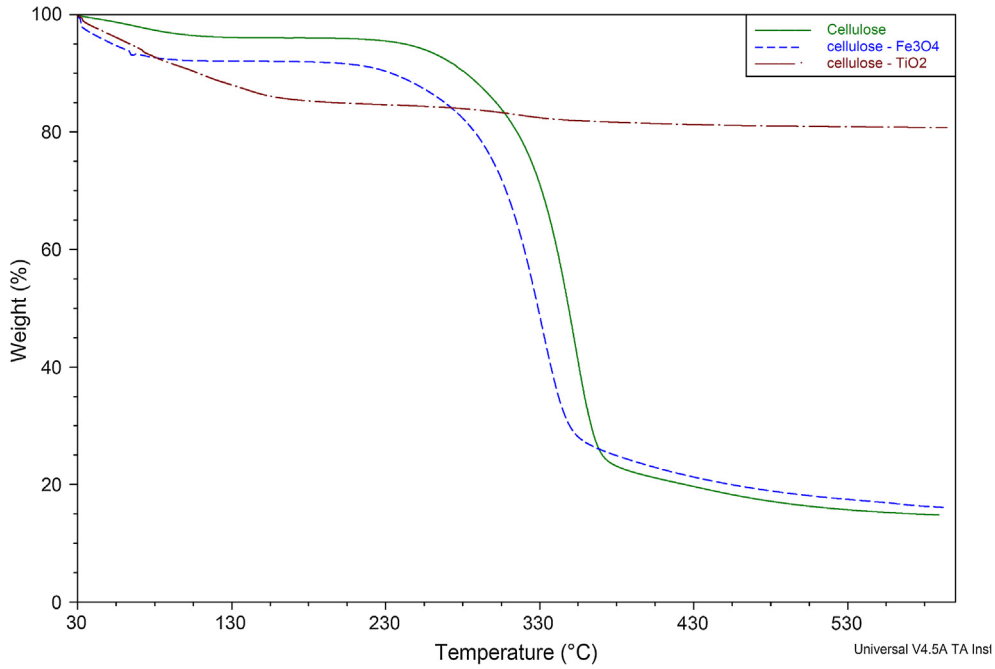

Fig. 5. TGA thermograms of cellulose and modified cellulose.

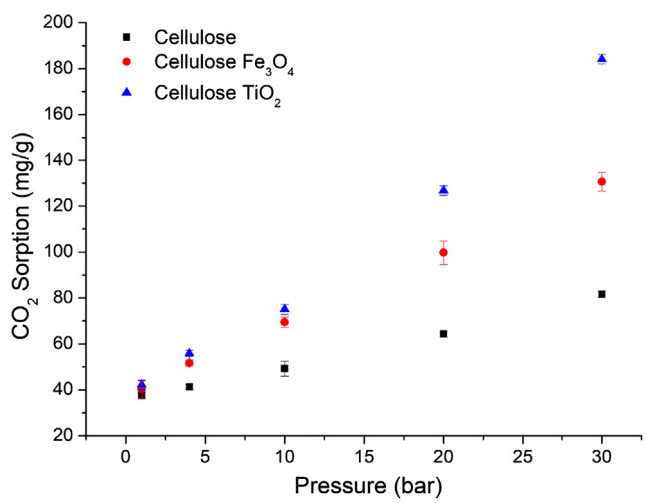

Fig. 6. CO_2 sorption for non-modified cellulose and modified samples at 298.15 K.

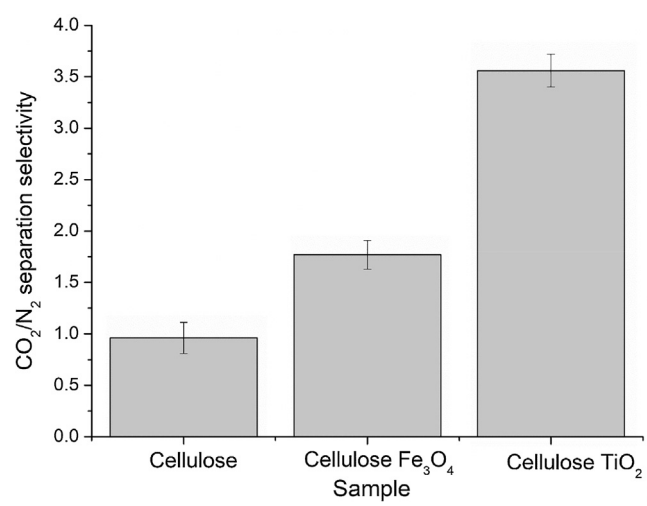

Fig. 8. CO_2/N_2 selectivity of non-modified cellulose and modified samples at 2 MPa and 298.15 K.

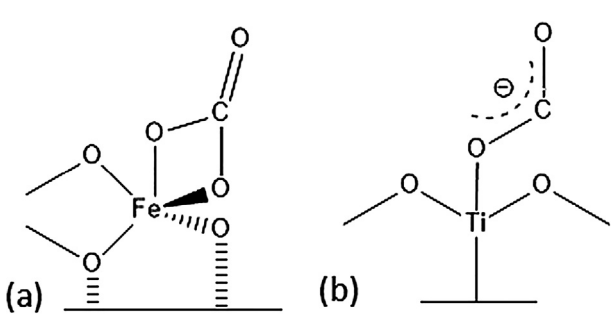

Fig. 7. Proposed acid-base adsorption mechanism of CO_2 onto modified cellulose: (a) cellulose-Fe_3O_4 and (b) cellulose-TiO_2.

oxides fragments occurs in the framework of Lewis acid-base theoretical description. Since the origin of interactions is the same, the corresponding adsorption energies are expectedly comparable. Somewhat stronger performance of anatase TiO_2 is due somewhat lower electronegativity of titanium, 1.63, as compared to iron, 1.88, and, therefore, somewhat larger partial point charges on the sorbent atoms that attract CO_2.

We cannot compare TiO_2 and Fe_3O_4 reinforcing agents directly due to very different content of them in our experimental samples. However, it is very clear from ab initio modeling that both additives are successful and that TiO_2 is somewhat better due to larger polarity of the Ti–O covalent bonds. Anatase TiO_2 is also more appealing than iron oxides thanks to its physical properties. Although a final product in the reaction of an acidic oxide and a basic oxide is a salt (metal carbonate), our reactions do not proceed so far, because proper heating was not attempted. The processes responsible for the experimentally observed CO_2 sorption values belong to instances of physical adsorption, including hydrogen bonding and acid-based attraction.

4. Conclusion

Cellulose was extracted from rice husk and modified with 0.4at.%

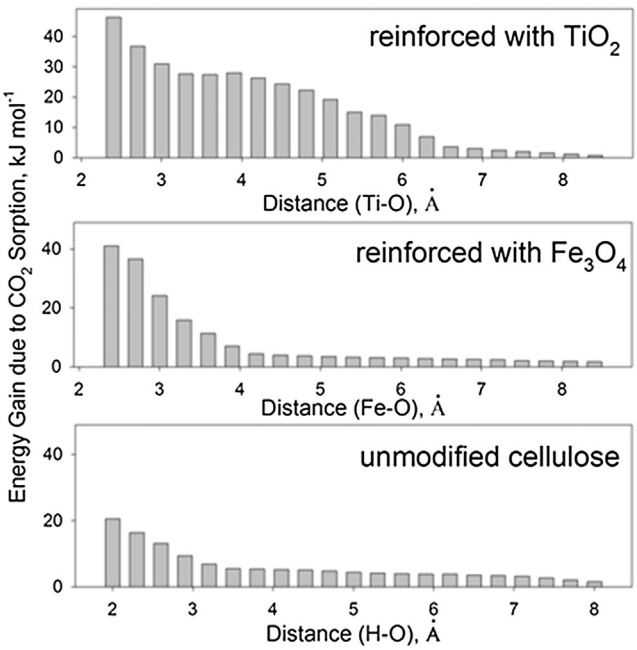

Fig. 9. Relative system energies as a function of sorbent-sorbate distance. The distances corresponding to the strongest atom-atom attraction in the system (in the sorbed state) were selected: titanium – oxygen, iron-oxygen, hydrogen – oxygen. The distances between the designated atom pairs increased stepwise until the energy gain due to interaction decreased to the geometry convergence threshold. The scale of all tabs was chosen identical for ease of comparison.

Fe Fe_3O_4 and 15.5at.% Ti anatase TiO_2 via hydroxyl group interactions. All three products were structurally confirmed through different characterization methods. The pressure decay technique provided evidence that both transition metal oxides Fe_3O_4 and TiO_2 increase the CO_2 sorption capacity and CO_2/N_2 selectivity of cellulose at all pressures, theoretically through acid-base interactions. Cellulose-TiO_2 shown a more important sorption increase of 125.6% at 30 bar and 12.2% at 1 bar compared to the increase of 8.0% at 1 bar and 60% at 30 bar provided by cellulose-Fe_3O_4. The Cellulose-TiO_2 showed the highest CO_2/N_2 selective capacity (3.56 ± 0.16). This suggests cellulose-TiO_2 provides the stronger adsorption interaction, but is most likely resultant of the higher at.% loading of the transition metal oxide when compared to cellulose-Fe_3O_4. To efficiently determine the most effective adsorbent an alternative modification method with a higher Fe loading at.% must be implemented. Due to their environmentally friendly nature and their proven CO_2 sorption ability, these compounds deserve more attention in this area of research.

Acknowledgments

The authors would like to thank Cooperativa Arrozeira Extremo Sul Ltda for donating rice husk and the Surface Science and Microscopy Laboratories (Guatiguará Technology Park - UIS) for XPS analysis. Sandra Einloft thanks CNPq for research scholarship.

References

[1] Parry ML, Canziani OF, Palutikof JP. Climate change 2007: Impacts, adaptation and vulnerability. Contribution of working group II to the fourth assessment report of the intergovernmental panel on climate change. Cambridge, UK: Cambridge University Press; 2007. p. 976.
[2] Songolzadeh M, Soleimani M, Takht Ravanchi M, Songolzadeh R. Carbon dioxide separation from flue gases: A technological review emphasizing reduction in greenhouse gas emissions. Sci World J 2014(2014). https://doi.org/10.1155/2014/828131.
[3] Abanades JC, Arias B, Lyngfelt A, Mattisson T, Wiley DE, Li H, et al. Emerging CO_2 capture systems. Int J Greenh Gas Control 2015;40:126–66. https://doi.org/10.1016/j.ijggc.2015.04.018.
[4] Flude S, Johnson G, Gilfillan SMV, Haszeldine RS. Inherent tracers for carbon capture and storage in sedimentary formations: composition and applications. Environ Sci Technol 2016;50:7939–55. https://doi.org/10.1021/acs.est.6b01548.
[5] Zhang Z, Xiao Y, Wang B, Sun Q, Liu H. Waste is a misplayed resource: synthesis of zeolites from fly ash for CO_2 capture. Energy Procedia 2017;114:2537–44. https://doi.org/10.1016/j.egypro.2017.08.036.
[6] Snider MT, Verweij H. Microporous and Mesoporous Materials Gas sorption studies on Zeolite Y membrane materials for post-combustion CO_2 capture in coal-fired plants. Microporous Mesoporous Mater 2014;192:3–7. https://doi.org/10.1016/j.micromeso.2013.10.022.
[7] Chen C, Zhang S, Ho K, Ahn W. Amine – silica composites for CO_2 capture: a short review. J Energy Chem 2017;26:868–80. https://doi.org/10.1016/j.jechem.2017.07.001.
[8] Zhang Z, Wang B, Sun Q, Ma X. Enhancing sorption performance of solid amine sorbents for CO_2 capture by additives. Energy Procedia 2013;37:205–10. https://doi.org/10.1016/j.egypro.2013.05.103.
[9] Ansaloni L, Rennemo R, Knuutila HK, Deng L. Development of membrane contactors using volatile amine-based absorbents for CO_2 capture : Amine permeation through the membrane. J Memb Sci 2017;537:272–82. https://doi.org/10.1016/j.memsci.2017.05.016.
[10] Duczinski R, Bernard F, Rojas M, Duarte E, Chaban V, Vecchia FD, et al. Waste derived MCMRH- supported IL for CO_2 /CH_4 separation. J Nat Gas Sci Eng 2018;54:54–64. https://doi.org/10.1016/j.jngse.2018.03.028.
[11] Zhao C, Guo Y, Li W, Bu C, Wang X, Lu P. Experimental and modeling investigation on CO_2 sorption kinetics over K_2CO_3 -modified silica aerogels. Chem Eng J 2017;312:50–8. https://doi.org/10.1016/j.cej.2016.11.121.
[12] Wang K, Shang H, Li L, Yan X. Efficient CO_2 capture on low-cost silica gel modified by polyethyleneimine. J Nat Gas Chem 2012;21:319–23. https://doi.org/10.1016/S1003-9953(11)60371-X.
[13] Yun Y, Sol H, Man J, Tae Y. Environmental Photocatalytic CO_2 conversion on highly ordered mesoporous materials : Comparisons of metal oxides and compound semiconductors. Appl Catal B Environ 2018;224:594–601. https://doi.org/10.1016/j.apcatb.2017.10.068.
[14] Chalal N, Bouhali H, Hamaizi H, Bengueddach A. CO_2 sorption onto silica mesoporous materials made from nonionic surfactants. Microporous Mesoporous Mater 2015;210:32–8. https://doi.org/10.1016/j.micromeso.2015.02.016.
[15] Einloft S, Bernard FL, Dalla Vecchia F. Chapter 17. Capturing CO_2 with Poly(Ionic Liquid)s. In: Eftekhari A, editor. Polym. Ion. Liq. 2017. p. 489–514. https://doi.org/10.1039/9781788010535-00489.
[16] Xing G, Zhang Y, Cao X. Bifunctional 3D porous Cu(I) metal-organic framework with gas sorption and luminescent properties. J Mol Struct 2017;1146:793–6. https://doi.org/10.1016/j.molstruc.2017.06.058.
[17] Gao F, Li Y, Ye Y, Zhao L. A robust microporous ytterbium metal-organic framework with open metal sites for highly selective adsorption of CO_2 over CH_4. Inorg Chem Commun 2017;86:137–9. https://doi.org/10.1016/j.inoche.2017.10.010.
[18] Zhao Y-P, Yang H, Wang F, Du Z-Y. A microporous manganese-based metal–organic framework for gas sorption and separation. J Mol Struct 2014;1074:19–21. https://doi.org/10.1016/j.molstruc.2014.05.033.
[19] López JM, Navarro MV, Murillo R, Grasa GS. Development of Synthetic Ca-based CO2 Sorbents for Sorption Enhanced Reforming Coupled to Ca/Cu Chemical Loop. Energy Procedia 2017;114:230–41. https://doi.org/10.1016/j.egypro.2017.03.1165.
[20] Yang Y, Liu W, Hu Y, Sun J, Tong X, Chen Q, et al. One-step synthesis of porous Li4SiO4-based adsorbent pellets via graphite moulding method for cyclic CO_2 capture. Chem Eng J 2018;353:92–9. https://doi.org/10.1016/j.cej.2018.07.044.
[21] Bernard FL, Duczinski RB, Rojas MF, Fialho MCC, Carreño LÁ, Chaban VV, et al. Cellulose based poly(ionic liquids): Tuning cation-anion interaction to improve carbon dioxide sorption. Fuel 2018;211:76–86. https://doi.org/10.1016/j.fuel.2017.09.057.
[22] Bernard FL, Rodrigues DM, Polesso BB, Donato AJ, Seferin M, Chaban VV, et al. New cellulose based ionic compounds as low-cost sorbents for CO_2 capture. Fuel Process Technol 2016;149:131–8. https://doi.org/10.1016/j.fuproc.2016.04.014.
[23] Klemm D, Heublein B, Fink H-P, Bohn A. Cellulose: fascinating biopolymer and sustainable raw material. Angew Chem Int Ed 2005;44:3358–93. https://doi.org/10.1002/anie.200460587.
[24] Ugheoke IB, Mamat O. A critical assessment and new research directions of rice husk silica processing methods and properties. Maejo Int J Sci Technol 2012;6:430–48. https://doi.org/10.14456/mijst.2012.31.
[25] Nascimento P, Marim R, Carvalho G, Celso R, Cid G, Celso R, et al. Nanocellulose produced from rice hulls and its effect on the properties of biodegradable starch film. Mater Res 2015;19:1–8. https://doi.org/10.1590/1980-5373-MR-2015-0423.
[26] Lau LC, Lee KT, Mohamed AR. Simultaneous SO_2 and NO removal using sorbents derived from rice husks: an optimisation study. Fuel 2011;90:1811–7. https://doi.org/10.1016/j.fuel.2010.12.009.
[27] Ferreira FV, Mariano M, Rabelo SC, Gouveia RF, Lona LMF. Isolation and surface modification of cellulose nanocrystals from sugarcane bagasse waste: From a micro- to a nano-scale view. Appl Surf Sci 2018;436:1113–22. https://doi.org/10.1016/j.apsusc.2017.12.137.
[28] El-Nahas AM, Salaheldin TA, Zaki T, El-Maghrabi HH, Marie AM, Morsy SM, et al. Functionalized cellulose-magnetite nanocomposite catalysts for efficient biodiesel production. Chem Eng J 2017;322:167–80. https://doi.org/10.1016/j.cej.2017.04.031.
[29] Yang J, Li J. Self-assembled cellulose materials for biomedicine: a review. Carbohydr Polym 2018;181:264–74. https://doi.org/10.1016/j.carbpol.2017.10.067.
[30] Liu H, Rong L, Wang B, Mao Z, Xie R, Xu H, et al. Facile synthesis of cellulose

derivatives based on cellulose acetoacetate. Carbohydr Polym 2017;170:117–23. https://doi.org/10.1016/j.carbpol.2017.04.043.
[31] Zhou L, He H, Li M-C, Huang S, Mei C, Wu Q. Grafting polycaprolactone diol onto cellulose nanocrystals via click chemistry: Enhancing thermal stability and hydrophobic property. Carbohydr Polym 2018;189:331–41. https://doi.org/10.1016/j.carbpol.2018.02.039.
[32] Chanapattharapol KC, Krachuamram S, Youngme S. Study of CO_2 adsorption on iron oxide doped MCM-41. Microporous Mesoporous Mater 2017;245:8–15. https://doi.org/10.1016/j.micromeso.2017.02.072.
[33] Su T, Qin Z, Huang G, Ji H, Jiang Y, Chen J. Density functional theory study on the interaction of CO_2 with Fe_3O_4 (111) surface. Appl Surf Sci 2016;378:270–6. https://doi.org/10.1016/j.apsusc.2016.03.097.
[34] Alfe M, Ammendola P, Gargiulo V, Raganati F, Chirone R. Magnetite loaded carbon fine particles as low-cost CO_2 adsorbent in a sound assisted fluidized bed. Proc Combust Inst 2015;35:2801–9. https://doi.org/10.1016/j.proci.2014.06.037.
[35] Jiang G, Huang Q, Kenarsari SD, Hu X, Russell AG, Fan M, et al. A new mesoporous amine-TiO_2 based pre-combustion CO_2 capture technology. Appl Energy 2015;147:214–23. https://doi.org/10.1016/j.apenergy.2015.01.081.
[36] Wang Q, Ma H, Chen J, Du Z, Mi J. Interfacial control of polyHIPE with nano-TiO_2 particles and polyethylenimine toward actual application in CO_2 capture. J Environ Chem Eng 2017;5:2807–14. https://doi.org/10.1016/j.jece.2017.05.034.
[37] Cao Y, Hu S, Yu M, Yan S, Xu M. Adsorption and interaction of CO_2 on rutile TiO_2 (110) surfaces: a combined UHV-FTIRS and theoretical simulation study. PCCP 2015;17:23994–4000. https://doi.org/10.1039/C5CP04013B.
[38] Li S-M, Dong Y-Y, Ma M-G, Fu L-H, Sun R-C, Xu F. Hydrothermal synthesis, characterization, and bactericidal activities of hybrid from cellulose and TiO_2. Carbohydr Polym 2013;96:15–20. https://doi.org/10.1016/j.carbpol.2013.03.058.
[39] Johar N, Ahmad I, Dufresne A. Extraction, preparation and characterization of cellulose fibres and nanocrystals from rice husk. Ind Crops Prod 2012;37:93–9. https://doi.org/10.1016/j.indcrop.2011.12.016.
[40] Zhong L, Fu S, Li F, Zhan H. Chlorine dioxide treatment of sisal fibre: Surface lignin and its influences on fibre surface characteristics and interfacial behaviour of sisal fibre/phenolic resin composites. BioResources 2010;5:2431–46. https://doi.org/10.1016/j.compositesa.2010.09.004.
[41] Segal L, Creely JJ, Martin AE, Conrad CM. An empirical method for estimating the degree of crystallinity of native cellulose using the X-ray diffractometer. Text Res J 1959;29:786–94. https://doi.org/10.1177/004051755902901003.
[42] Koros WJ, Paul DR. Design considerations for measurement of gas sorption in polymers by pressure decay. J Polym Sci Polym Phys Ed 1976;14:1903–7. https://doi.org/10.1002/pol.1976.180141014.
[43] Bernard FL, Polesso BB, Cobalchini FW, Chaban VV, do Nascimento JF, Dalla Vecchia F, Einloft S. Hybrid alkoxysilane-functionalized urethane-imide-based poly (ionic liquids) as a new platform for carbon dioxide capture. Energy Fuels 2017;31:9840–9. https://doi.org/10.1021/acs.energyfuels.7b02027.
[44] Span W, Wagner R. A new EOS for CO_2 covering the fluid region from the triple point temperature to 1100K at pressures up to 800MPa.pdf. J Phys Chem Ref Data 1996;25:1509–96. https://doi.org/10.1063/1.555991.
[45] Fernández Rojas M, Pacheco Miranda L, Martinez Ramirez A, Pradilla Quintero K, Bernard F, Einloft S, Carreño Díaz LA. New biocomposites based on castor oil polyurethane foams and ionic liquids for CO_2 capture. Fluid Phase Equilib 2017;452:103–12. https://doi.org/10.1016/j.fluid.2017.08.026.
[46] Azimi A, Mirzaei M. Experimental evaluation and thermodynamic modeling of hydrate selectivity in separation of CO_2 and CH_4. Chem Eng Res Des 2016;111:262–8. https://doi.org/10.1016/j.cherd.2016.05.005.
[47] Peverati R, Truhlar DG. Performance of the M11 and M11-L density functionals for calculations of electronic excitation energies by adiabatic time-dependent density functional theory. PCCP 2012;14:11363. https://doi.org/10.1039/c2cp41295k.
[48] Hay PJ, Wadt WR. Ab, initio effective core potentials for molecular calculations. Potentials for K to Au including the outermost core orbitals. J Chem Phys 1985;82:299–310. https://doi.org/10.1063/1.448975.
[49] Grimme S, Antony J, Ehrlich S, Krieg H. A consistent and accurate ab initio parametrization of density functional dispersion correction (DFT-D) for the 94 elements H-Pu. J Chem Phys 2010;132:154104https://doi.org/10.1063/1.3382344.
[50] Schmidt MW, Baldridge KK, Boatz JA, Elbert ST, Gordon MS, Jensen JH, et al. General atomic and molecular electronic structure system. J Comput Chem 1993;14:1347–63. https://doi.org/10.1002/jcc.540141112.
[51] Klemm D, Kramer F, Moritz S, Lindström T, Ankerfors M, Gray D, et al. Nanocelluloses: a new family of nature-based materials. Angew Chemie Int Ed 2011;50:5438–66. https://doi.org/10.1002/anie.201001273.
[52] Das C, Gebru KA. Cellulose acetate modified titanium dioxide (TiO_2) nanoparticles electrospun composite membranes: fabrication and characterization. J Inst Eng Ser E 2017;98:91–101. https://doi.org/10.1007/s40034-017-0104-1.
[53] Marques PAAP, Trindade T, Neto CP. Titanium dioxide/cellulose nanocomposites prepared by a controlled hydrolysis method. Compos Sci Technol 2006;66:1038–44. https://doi.org/10.1016/j.compscitech.2005.07.029.
[54] An X, Cheng D, Dai L, Wang B, Ocampo HJ, Nasrallah J, et al. Synthesis of nanofibrillated cellulose/magnetite/titanium dioxide (NFC@Fe_3O_4 @TNP) nanocomposites and their application in the photocatalytic hydrogen generation. Appl Catal B Environ 2017;206:53–64. https://doi.org/10.1016/j.apcatb.2017.01.021.
[55] Xia W, Yin C, Wang F, Li J, Wei X. Preparation and characterization of Fe_3O_4/cellulose composite material by the method of solidoid compound. Int Symp Energy Sci Chem Eng (ISESCE 2015) 2015:100–3.
[56] Liu CF, Zhang AP, Li WY, Yue FX, Sun RC. Succinoylation of cellulose catalyzed with iodine in ionic liquid. Ind Crops Prod 2010;31:363–9. https://doi.org/10.1016/j.indcrop.2009.12.002.
[57] Ciolacu D, Ciolacu F, Popa VI. Amorphous cellulose – structure and characterization. Cellul Chem Technol 2011;45:13–21. https://doi.org/10.1163/156856198X00740.
[58] Namdeo M, Bajpai SK. Immobilization of α-amylase onto cellulose-coated magnetite (CCM) nanoparticles and preliminary starch degradation study. J Mol Catal B Enzym 2009;59:134–9. https://doi.org/10.1016/j.molcatb.2009.02.005.
[59] Shahid MK, Phearom S, Choi Y-G. Synthesis of magnetite from raw mill scale and its application for arsenate adsorption from contaminated water. Chemosphere 2018;203:90–5. https://doi.org/10.1016/j.chemosphere.2018.03.150.
[60] Wang P, Zhan S, Xia Y, Ma S, Zhou Q, Li Y. The fundamental role and mechanism of reduced graphene oxide in rGO/Pt-TiO_2 nanocomposite for high-performance photocatalytic water splitting. Appl Catal B Environ 2017;207:335–46. https://doi.org/10.1016/j.apcatb.2017.02.031.
[61] Sun D, Yang J, Wang X. Bacterial cellulose/TiO_2 hybrid nanofibers prepared by the surface hydrolysis method with molecular precision. Nanoscale 2010;2:287–92. https://doi.org/10.1039/B9NR00158A.
[62] Samadi A, Kemmerlin RK, Husson SM. Polymerized Ionic Liquid Sorbents for CO2 Separation. Energy Fuels 2010;1:5797–804. https://doi.org/10.1021/ef101027s.
[63] Wang X, Lu Z, Jia L, Chen J. Physical properties and pyrolysis characteristics of rice husks in different atmosphere. Results Phys 2016;6:866–8. https://doi.org/10.1016/j.rinp.2016.09.011.
[64] Tursi A, Beneduci A, Chidichimo F, De Vietro N, Chidichimo G. Remediation of hydrocarbons polluted water by hydrophobic functionalized cellulose. Chemosphere 2018;201:530–9. https://doi.org/10.1016/j.chemosphere.2018.03.044.
[65] Idczak K, Idczak R, Konieczny R. An investigation of the corrosion of polycrystalline iron by XPS, TMS and CEMS. Phys B Condens Matter 2016;491:37–45. https://doi.org/10.1016/j.physb.2016.03.018.
[66] Huong PTL, Huy LT, Lan H, Thang LH, An TT, Van Quy N, et al. Magnetic iron oxide-carbon nanocomposites: Impacts of carbon coating on the As(V) adsorption and inductive heating responses. J Alloy Compd 2018;739:139–48. https://doi.org/10.1016/j.jallcom.2017.12.178.
[67] Liu H, Wei G, Xu Z, Liu P, Li Y. Quantitative analysis of Fe and Co in Co-substituted magnetite using XPS: The application of non-linear least squares fitting (NLLSF). Appl Surf Sci 2016;389:438–46. https://doi.org/10.1016/j.apsusc.2016.07.146.
[68] Wilson D, Langell MA. XPS analysis of oleylamine/oleic acid capped Fe3O4 nanoparticles as a function of temperature. Appl Surf Sci 2014;303:6–13. https://doi.org/10.1016/j.apsusc.2014.02.006.
[69] Yang S, Xiong Y, Ge Y, Zhang S. Heterogeneous Fenton oxidation of nitric oxide by magnetite: Kinetics and mechanism. Mater Lett 2018;218:257–61. https://doi.org/10.1016/j.matlet.2018.01.171.
[70] Kerber SJ, Bruckner JJ, Wozniak K, Seal S, Hardcastle S, Barr TL. The nature of hydrogen in x-ray photoelectron spectroscopy: General patterns from hydroxides to hydrogen bonding. J Vac Sci Technol A Vacuum, Surfaces, Film 1996;14:1314–20. https://doi.org/10.1116/1.579947.
[71] Sánchez-Rodríguez D, Méndez Medrano MG, Remita H, Escobar-Barrios V. Photocatalytic properties of BiOCl-TiO_2 composites for phenol photodegradation. J Environ Chem Eng 2018;6:1601–12. https://doi.org/10.1016/j.jece.2018.01.061.
[72] Wang W, Liang T, Bai H, Dong W, Liu X. All cellulose composites based on cellulose diacetate and nanofibrillated cellulose prepared by alkali treatment. Carbohydr Polym 2018;179:297–304. https://doi.org/10.1016/j.carbpol.2017.09.098.
[73] Oliveira AC de M, dos Santos MS, Brandão LMS, de Resende ITF, Leo IM, Morillo ES, Yerga RMN, Fierro JLG, Egues SM da S, Figueiredo RT. The effect of cellulose loading on the photoactivity of cellulose-TiO_2 hybrids for hydrogen production under simulated sunlight. Int J Hydrogen Energy 2017;42:28747–54. https://doi.org/10.1016/j.ijhydene.2017.09.022.
[74] Heo US, Kim D-W, Kim K-S, Park D-W. A facile synthesis of anatase TiO_2 -Graphene nanocomposites using plasma and heat treatment. Appl Surf Sci 2018. https://doi.org/10.1016/j.apsusc.2018.04.083.
[75] Haider AJ, ALAnbari RH, Kadhim GR, Salame CT. Exploring potential Environmental applications of TiO_2 Nanoparticles. Energy Procedia 2017;119:332–45. https://doi.org/10.1016/j.egypro.2017.07.117.
[76] Zhang Y-HP, Lynd LR. Toward an aggregated understanding of enzymatic hydrolysis of cellulose: noncomplexed cellulase systems. Biotechnol Bioeng 2004;88:797–824. https://doi.org/10.1002/bit.20282.
[77] Collazo-Bigliardi S, Ortega-Toro R, Chiralt Boix A. Isolation and characterisation of microcrystalline cellulose and cellulose nanocrystals from coffee husk and comparative study with rice husk. Carbohydr. Polym 2018;191:205–15. https://doi.org/10.1016/j.carbpol.2018.03.022.
[78] Naduparambath S, Jinitha TV, Shaniba V, Sreejith MP, Balan Aparna K, Purushothaman E. Isolation and characterisation of cellulose nanocrystals from sago seed shells. Carbohydr Polym 2018;180:13–20. https://doi.org/10.1016/j.carbpol.2017.09.088.
[79] Challagulla S, Tarafder K, Ganesan R, Roy S. Structure sensitive photocatalytic reduction of nitroarenes over TiO_2. Sci Rep 2017;7:8783. https://doi.org/10.1038/s41598-017-08599-2.
[80] Wang Z, Mao L, Lin J. Preparation of TiO_2 nanocrystallites by hydrolyzing with gaseous water and their photocatalytic activity. J Photochem Photobiol A Chem 2006;177:261–8. https://doi.org/10.1016/j.jphotochem.2005.06.005.
[81] Djordjevic N, Marinkovic A, Nikolic J, Drmanic S, Rancic M, Brkovic D, Uskokovic P. A study of the barrier properties of polyethylene coated with nanocellulose/magnetite composite film. J Serbian Chem Soc 2016. https://doi.org/10.2298/JSC151217019D. 19–19.
[82] Du Q, Ma T, Fu C, Liu T, Huang Z, Ren J, et al. Encapsulating ionic liquid and Fe_3O_4 nanoparticles in gelatin microcapsules as microwave susceptible agent for MR imaging-guided tumor thermotherapy. ACS Appl Mater Interfaces 2015;7:13612–9. https://doi.org/10.1021/acsami.5b03230.

[83] Chowdhury S, Parshetti GK, Balasubramanian R. Post-combustion CO_2 capture using mesoporous TiO_2 /graphene oxide nanocomposites. Chem Eng J 2015;263:374–84. https://doi.org/10.1016/j.cej.2014.11.037.
[84] Gabrienko AA, Ewing AV, Chibiryaev AM, Agafontsev AM, Dubkov KA, Kazarian SG. New insights into the mechanism of interaction between CO_2 and polymers from thermodynamic parameters obtained by in situ ATR-FTIR spectroscopy. PCCP 2016;18:6465–75. https://doi.org/10.1039/C5CP06431G.
[85] Tomasko DL, Li H, Liu D, Han X, Wingert MJ, Lee LJ, et al. A Review of CO_2 Applications in the Processing of Polymers. Ind Eng Chem Res 2003;42:6431–56. https://doi.org/10.1021/ie030199z.